DOI: 10.61782/fa.2025.0927

FORUM ACUSTICUM EURONOISE 2025

ULTRASONIC MAGING OF LAYER ON SUBSTRATE STRUCTURES USING HIGH-FREQUENCY ACOUSTIC FIELD CORRELATION

Nada Ben Jafela Lynda Chehami* Marc Duquennoy Emmanuel Moulin
Nikolay Smagin Dame Fall Zakariae Oumekloul

UPHF, CNRS, univ. Lille, UMR 8520-IEMN, F-59313, Valenciennes, France

ABSTRACT

Layer on substrate structures are often subject to various types of defects, particularly those resulting from manufacturing process during thin-film growth. Currently, one method of inspecting such structures involves the use of IDT transducers for excitation and laser vibrometry for reception. In this work, we propose a complementary approach inspired by passive noise correlation imaging methods initially developed in geophysics. This technique is applied here to image layered structures on substrates by exploiting the correlation of diffuse acoustic waves and the associated principle of passive Green's function reconstruction, enabling the detection and imaging of defects. The analysis was performed using numerical simulations and preliminary experiments on silicon wafers (3 mm thick). IDTs (10-25) MHz were used to generate surface waves, and the resulting displacement field was captured using laser vibrometry. Simulations and measurements were carried out on both defect-free and defect-containing cases. Correlation matrices were calculated on Full Matrix Capture mode. Finally, a beamforming algorithm was applied to localize defects, taking into account silicon's anisotropy.

Keywords: *Ultrasonic imaging, beamforming, anisotropy, Noise correlation, SAW, IDT.*

1. INTRODUCTION

Layer-On-Substrate (LOS) structures are subject to numerous degradations related to: manufacturing defects during thin film growth (thickness gradient), the quality of layer adhesion to the substrate (surface roughness), cracks, and delaminations. For these reasons, the microelectronics industry is increasingly interested in non-destructive evaluation methods, particularly for characterizing bonding quality in wafer assemblies. The work presented here proposes an alternative method based on the correlation of diffuse surface acoustic waves generated by inter-digital transducers (IDTs) operating in the frequency band between 10 and 25 MHz.

Typically, LOS characterization using IDT is performed by emitting a short (broadband) pulse onto the sample to be inspected, whose vibrational displacement amplitudes are then measured by a laser vibrometer. At high frequencies, this procedure must be performed with high precision, making automation a challenge. This so-called active method has yielded very promising results for the characterization of thin layers such as sol-gels [1, 2].

Meanwhile, the acoustic field correlation approach, initially used in geophysical applications [3–6] or in underwater acoustics [7–9], provides a relevant theoretical basis for the passive reconstruction of the medium's impulse response known as the Green's function (GF). Generally, GF estimation by noise correlation is based on the principle that waves emitted by random noise sources, when recorded at two points in the medium, can be used to retrieve the impulse response of the medium between these points sensing. In other words, the cross-correlation $C_{AB}(t)$ of the signals recorded at these two points A and B makes it possible to reconstruct the impulse response of the medium :

$$\frac{\partial}{\partial t} C_{AB}(t) = K\ [G_{AB}(t) - G_{AB}(-t)] + n_{AB}(t) \quad (1)$$

where C_{AB} is the cross-correlation between points A and B of the medium, G_{AB} is the Green's function (GF) between the same points, K is a constant depending on the properties of the medium and the noise source, and n_{AB} is the residual error of the GF reconstruction.

This method is particularly useful in situations where it is difficult to generate controlled signals, such as in seismology, aeronautics, etc. However, the reconstruction quality is particularly influenced by the way the sources are distributed (localized or not), the number of sources, and the nature of the medium (absorption, attenuation, scattering, reverberation) [10]. In NDT/SHM, this method has been successfully validated at low frequencies (10, 30) kHz (Lamb waves) on aluminum damaged plates (cracks, holes, etc.) [11, 12].

In this work, we propose to extend this method to high frequencies (5-25) MHz by exploiting surface waves to probe microstructures (silicon wafers). Although complex (due to anisotropy), we first propose a simple numerical study to validate the approach on an anisotropic medium, and then it was attempted experimentally by developing suitable instrumentation using IDTs. Although promising, IDTs have rather poor reception capabilities; we therefore propose to use them here as a source of diffuse surface acoustic waves. IDTs are fabricated to focus the energy of surface acoustic waves onto the entire wafer [13]. To take full advantage of this method, optical detection is used and correlation functions are calculated. Figure 1 illustrates this principle.

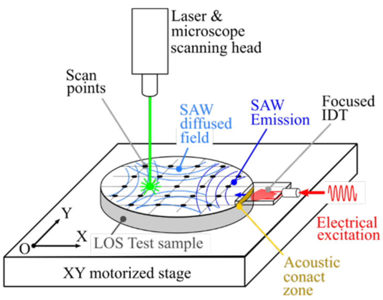

Figure 1. Schematic representation of the proposed characterization method based on the diffuse acoustic wave correlation.

The paper is divided into three parts: Section (1) is dedicated to the imaging in silicon (100); Section (2) is dedicated to numerical validation; and Section (3) is dedicated to the development of the instrumentation and preliminary tests on the GF reconstruction. Finally, a conclusion and perspectives.

2. IMAGING IN ANISOTROPIC MEDIA USING SURFACE WAVES

2.1 SAW propgation in Silicon (100)

Surface Acoustic Waves (SAW) propagate parallel to the surface of an elastic material, and their amplitude decreases rapidly, often exponentially, through the depth of the material. The penetration depth is of the order of the wavelength, providing high sensitivity to surface defects, voids, cracks, coatings, films, and nano/microparticles adhering to the surface. These waves are currently attracting increasing interest, particularly for miniaturization aspects. However, the acoustic propagation of these waves in anisotropic media is complex, where velocities depend on the propagation direction. Several theoretical studies [14, 15] are devoted to determining an analytical formulation of velocity profiles in anisotropic materials. In this paper, the velocities are calculated numerically using the analytical equation proposed by Teransako et al. [16].

On can recall here the Hooke's law extended to anisotropic materials using a tensor formulation that includes orientation:

$$\sigma_{ij} = c_{ijkl}\,\epsilon_{kl}; \quad i, j, k, l = 1, 2, 3 \tag{2}$$

where σ and ϵ are the stress and strain tensors.

The general case of a fourth-rank tensor requires 81 terms. By exploiting the cubic symmetry properties (silicon (100) has a face-centered diamond cubic crystallographic structure), the anisotropic properties of a cubic crystal can be described with a 6×6 matrix using a simplified tensor notation, which requires only three independent values: $c_{11} = 165.7$ GPa, $c_{12} = 63.9$ GPa, and $c_{44} = 79.56$ GPa.

The physical properties of silicon (100) are: Poisson's ratio $\nu = \frac{c_{12}}{c_{11}+c_{12}} = 0.278$; Young's modulus $E = c_{11} - 2\nu c_{12} = 130$ GPa; density $\rho = 2330$ kg/m^3; and the Zener coefficient $Z = \frac{2c_{44}}{c_{11}-c_{12}} = 1.56$.

In our case, the material under test is considered as a semi-infinite volume. Fig. 2 shows the estimated speed profile.

Two modes are observed for surface waves (regular mode and pseudo-mode) over a velocity range of 4500 to 5500 m/s.

In the following subsection, to perform defect imaging, an interpolation was performed on the two observed modes.

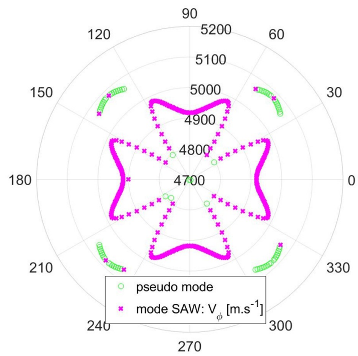

Figure 2. Theoretical (background) and experimental (red dots) velocity profiles.

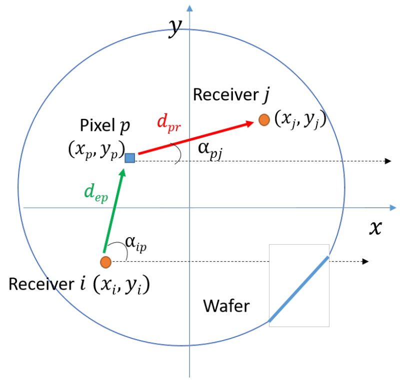

Figure 3. Illustration of the beamforming algorithm in anisotropic medium (backpropagation).

2.2 Imaging in anisotropic material

Considering two receivers R_i and R_j, the cross-correlation of the recorded signals across N_s noise sources can be expressed as follows:

$$C_{ijN_{Ns}}(\omega) = N_s\, D_{ij}(\omega) + n_{ijN_s}(\omega) \tag{3}$$

where D_{ij} represents a deterministic term containing the causal and anti-causal parts of the Green's function between the two receiver positions, and n_{ijN_s} is a term related to the residual noise from the reconstruction of the Green's function. As in [17], we adopt the differential beamforming algorithm to extract the defect signature, i.e., $\Delta\mathbf{C} = \mathbf{C}^{def} - \mathbf{C}^{ref}$, where "def" and "ref" refer to the cases with and without defects, respectively.

The principle consists of taking the image element index $(i{,}j)$ of the matrix $\Delta\varphi$ and backpropagating it according to the current position of the pixel (x_p, y_p) and for each propagation direction (see Fig. 3). Concretely, this consists of multiplying the differential matrix by a phase function involving the wave number k depending on the surface wave direction, i.e.

$$bpf_(x_p, y_p)(\omega) = \sum_{i=1,\,j=1}^{N,N} \Delta\mathbf{C_{ij}}(\omega)\, e^{[+j\,k(\omega,\alpha_{ip})\,d_{ip}+k(\omega,\alpha_{pj})\,d_{pj}]} \tag{4}$$

with $\alpha_{ip} = atan\left|\frac{y_p - y_i}{x_p - x_i}\right|$ and $\alpha_{pj} = \arctan\left|\frac{y_j - y_p}{x_j - x_p}\right|$. The terms d_{ip} and d_{pj} are the distances from receiver i to pixel and from pixel to receiver j, respectively.

After returning to the time domain using an inverse Fourier transform, the pixel intensity is obtained by summing the resulting waveforms for each index value $(i,\, j)$ and calculating the energy of this sum over a time window T_0 (typically the inverse of the bandwidth):

$$I(x,y) = \int_0^{T_0} [bpf_{(x_p,y_p)}(t)]^2, dt, \tag{5}$$

where $bpf(t)$ is the FT of $bpf(\omega)$.

For pixels located on the defect, this amounts to a constructive sum and therefore to a maximum intensity at the defect position.

In Section 3, a numerical validation was proposed.

3. NUMERICAL VALIDATION

To validate the imaging algorithm proposed for anisotropic media, a simplified numerical simulation is proposed.

We consider the propagation of surface waves in an infinite plate without absorption. In the frequency domain, this propagation between a source and a receiver R_i at positions $\vec{r_s}$ and $\vec{r_i}$, respectively, can be modeled in the far field using the propagation function defined as follows:

$$P(\vec{r_s}, \vec{r_i}, \omega) = \frac{1}{\sqrt{(\vec{r_s} - \vec{r_i})}}\, e^{[-j\,k(\omega,\alpha_{ip})\,d_{ip}+k(\omega,\alpha_{pj})\,d_{pj}.]} \tag{6}$$

Therefore, the signal received at R_i can be expressed as follows:

$$u(\vec{r_s}, \vec{r_i}, \omega) = P(\vec{r_s}, \vec{r_i}, \omega)\, u_e(\omega), \quad (7)$$

where $u_e(\omega)$ is the Fourier transform of the transmitted signal.

In the presence of a defect, the signal received at R_i can be written as follows:

$$u_d(\vec{r_s}, \vec{r_i}, \omega) = u(\vec{r_s}, \vec{r_i}, \omega) + \Delta u(\vec{r_s}, \vec{r_i}, \omega), \quad (8)$$

with $\Delta u(\omega) = f_d(\omega)\, P(\omega)\, u(\omega)$. Here f_d represents the defect scattering amplitude and $\vec{r_d}$ is the defect position.

Using the inverse Fourier transform, we return to the time domain to obtain the signals $u_d(t)$ and $u(t)$ received by R_i in both cases: with and without a defect, respectively.

The tested configuration consists of an infinite silicon wafer whose properties are implicitly introduced in the previously estimated dispersion curves. Twelve receivers (crosses) are placed at known positions on its surface. The origin is taken at the low left corner of the wafer. At the center of the imaging array, a defect is modeled by a point scatterer of constant f_d (isotropic scatterer). A set of 361 sources (red dots) are randomly distributed around the receivers.

The transmission signal is a sinusoidal cycle weighted by a Hanning window at a center frequency of 7 MHz. The sampling rate is 300 MS/s. The signals are acquired for 28 μs. For each pair of receivers, the summed cross-correlation across all sources is calculated. The back-propagation-based imaging algorithm discussed above is then applied to the positive-time correlations. The localization image obtained for an area of (45 $\times$ 45) cm2 around the defect is shown in Fig. 4 for active and passive cases.

Pixel intensities are normalized relative to the maximum intensity. As observed, the defect location is correctly localized in passive mode compared to active result.

In what follows, we propose a suitable instrumentation to validate these numerical results.

4. EXPERIMENTAL VALIDATION: ESTIMATION OF GREEN'S FUNCTIONS

Here, we initially focused on studying correlation functions in a "defect-free" case. The experiments were performed on a silicon wafer of 7 cm in diameter and 2 mm

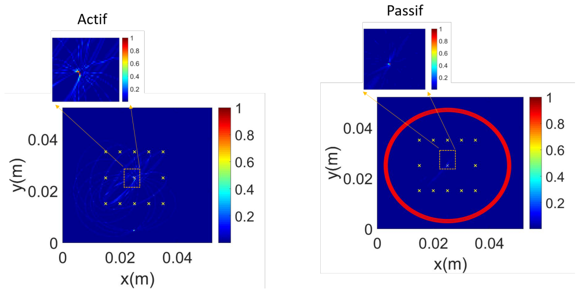

Figure 4. Defect localization image in active (raw signals in FMC mode) and passive (correlation functions, red circles indicate source positions) configurations.

thick. Surface acoustic waves were generated using a 7 to 25 MHz IDT transducer designed for this study [13], oriented at 45 degrees to favor the radiation of Rayleigh waves and minimize their conversion into bulk waves radiating into the substrate (cf Fig. 5). Since the transducer aperture is approximately 2 mm, the measurement points were chosen within the IDT's radiation zone. The measurement step size was approximately 10 mm, and a measurement grid of N = 25 points was created. Each Ascan is averaged 350 times and recorded over 2 ms. This corresponds to approximately 1000 times the reverberation time in the wafer.

The correlation functions are then calculated, and we obtain N$\times$ N impulse responses. Figure 6 shows a seismogram of cross-correlations between measurement point 3 of the grid and the other points on the same line.

As can be seen, the correlation functions are not symmetrical at zero. This demonstrates poor reconstruction quality of the Green's function (generally, when the correlation function is symmetrical between positive and negative times, it is a good indicator of convergence towards the Green's function). This can be explained by the fact that surface waves are not sufficiently reverberant at these operating frequencies. Another phenomenon may also occur, such as the conversion of surface wave modes into bulk waves. This work is in progress.

5. CONCLUSION

In conclusion, this study has shown the interest of the passive approach by correlation of diffuse waves to image silicon wafers. The results obtained by the numerical simulation are promising and have allowed to validate the

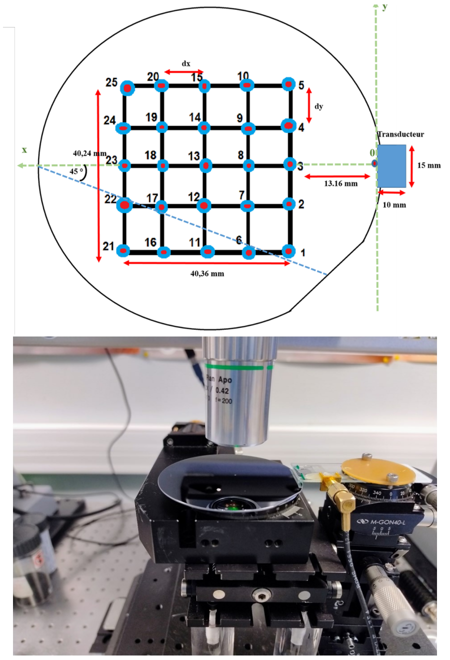

Figure 5. Experimental setup.

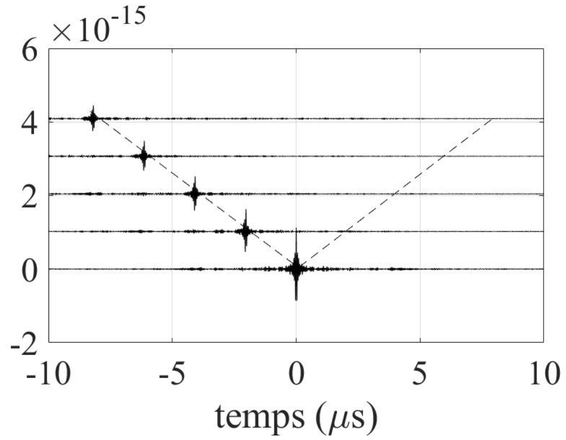

Figure 6. Seismogram of cross-correlations between measurement point 3 and the other points on the same line (see Fig. 5).

imaging algorithm in anisotropic medium. An experimental study was also conducted where an instrumentation adapted to generate a high frequency diffuse field by interdigital transducers was proposed. A preliminary study was first carried out on the estimation of the Green functions on a healthy wafer (without defect). The first results clearly show that surface waves are not very reverberant at these frequency ranges. To image micro-structures it is necessary to consider lower frequencies while remaining at the MHz scale, which can be particularly interesting in particular to image bonding defects in wafers. This approach certainly has a strong potential in the field of microelectronics.

6. ACKNOWLEDGMENTS

This project is funded by the French National Research Agency (ANR): DACLOS N^0:ANR-21-CE42-0002-01.

7. REFERENCES

[1] D. Fall, M. Duquennoy, M. Ouaftouh, N. Smagin, B. Piwakowski, and F. Jenot, “Non-destructive characterization of surfaces and thin coatings using a large-bandwidth interdigital transducer,” *Review of Scientific Instruments*, vol. 89, Dec. 2018.

[2] D. Fall, F. Compoint, M. Duquennoy, H. Piombini, M. Ouaftouh, F. Jenot, B. Piwakowski, P. Belleville, and C. Ambard, “Surface acoustic wave characterization of optical sol-gel thin layers,” *Ultrasonics*, vol. 68, pp. 102–107, may 2016.

[3] N. Shapiro, M. Campillo, L. Stehly, and M. Ritzwoller, “High-resolution surface-wave tomography from ambient seismic noise,” *Science*, vol. 29, pp. 1615–1617, 2005.

[4] Y. Zheng, “Retrieving the exact Green’s function by wavefield crosscorrelation,” *The Journal of the Acoustical Society of America*, vol. 127, pp. EL93–EL98, mar 2010.

[5] K. Wapenaar, D. Draganov, R. Snieder, X. Campman, and A. Verdel, “Tutorial on seismic interferometry: Part 1 — basic principles and applications,” *GEOPHYSICS*, vol. 75, pp. 75A195–75A209, sep 2010.

[6] Y. Chen and E. Saygin, “Green’s function retrieval from deterministic seismic wavefield using higher-order cross-correlation,” *ASEG Extended Abstracts*, vol. 2019, pp. 1–5, nov 2019.

[7] P. Roux and M. Fink, “Green’s function estimation using secondary sources in a shallow water environment,” *The Journal of the Acoustical Society of America*, vol. 113, pp. 1406–1416, mar 2003.

[8] V. V. Goncharov, Y. A. Chepurin, and O. A. Godin, "Passive acoustic tomography of the ocean using arrays of unknown shape," *Acoustical Physics*, vol. 59, pp. 170–178, mar 2013.

[9] M. G. Brown, O. A. Godin, N. J. Williams, N. A. Zabotin, L. Zabotina, and G. J. Banker, "Acoustic Green's function extraction from ambient noise in a coastal ocean environment," *Geophysical Research Letters*, vol. 41, pp. 5555–5562, aug 2014.

[10] L. Chehami, E. Moulin, J. de Rosny, and C. Prada, "Accuracy of green's function estimation from correlation of diffuse elastic waves on thin plates," *The Journal of the Acoustical Society of America*, vol. 146, pp. 3505–3511, nov 2019.

[11] L. Chehami, J. de Rosny, C. Prada, E. Moulin, and J. Assaad, "Experimental study of passive defect localization in plates using ambient noise," *IEEE Transactions on Ultrasonics, Ferroelectrics, and Frequency Control*, vol. 62, pp. 1544–1553, aug 2015.

[12] L. Chehami, E. Moulin, J. de Rosny, C. Prada, E. Chatelet, G. Lacerra, K. Gryllias, and F. Massi, "Nonlinear secondary noise sources for passive defect detection using ultrasound sensors," *Journal of Sound and Vibration*, vol. 386, pp. 283–294, jan 2017.

[13] M. Duquennoy, D. Fall, N. Ben Jafela, N. Smagin, Z. Oumekloul, L. Chehami, E. Moulin, and M. Ouaftouh, "A comparative study of divergent surface acoustic wave beams' generation on an y128° lithium niobate using various types of interdigital transducers," *Sensors*, vol. 25, p. 1067, Feb. 2025.

[14] G. Farnell, *Properties of elastic surface waves*. McGille University, 1969.

[15] Y. L. Y. X. D. Q. B. W. C. H. Guorong Song, Guangfu Hong, "Inversion of elastic constants of anisotropic (100) silicon based on surfacewave velocity by acoustic microscopy using particle swarm-based-simulated annealing optimization," *J Nondestruct Eval*, p. 34:43, 2015.

[16] A. T. R. C. nd Radim Kudelka, "Theoretical and experimental revision of surface acoustic waves on the (100) plane of silicon," *Scientific Reports*, vol. 11, no. 1, p. 2845, 2021.

[17] L. Chehami, E. Moulin, J. de Rosny, C. Prada, O. B. Matar, F. Benmeddour, and J. Assaad, "Detection and localization of a defect in a reverberant plate using acoustic field correlation," *Journal of Applied Physics*, vol. 115, p. 104901, mar 2014.